Title

A polymer-free, biomimicry drug self-delivery system fabricated via a synergistic combination of bottom-up and top-down approaches

Journal

Journal of Materials Chemistry B, 6(47)

ISSN

2050-750X

Authors

Xu, Xiaobao
Yang, Gaomai
Xue, Xiangdong
et al.

Publication Date

2018-12-21

DOI

10.1039/c8tb01464g

Peer reviewed

HHS Public Access

Author manuscript

J Mater Chem B. Author manuscript; available in PMC 2019 December 21.

Published in final edited form as:

J Mater Chem B. 2018 December 21; 6(47): 7842–7853. doi:10.1039/C8TB01464G.

A polymer-free, biomimicry drug self-delivery system fabricated via a synergistic combination of bottom-up and top-down approaches

Xiaobao Xu[#a,b,c], **Gaomai Yang**[#c], **Xiangdong Xue**[c], **Hongwei Lu**[c], **Hao Wu**[c], **Yee Huang**[d], **Di Jing**[c], **Wenwu Xiao**[c], **Jingkui Tian**[a], **Wei Yao**[b], **Chong-xian Pan**[b], **Tzu-yin Lin**[b,*], **Yuanpei Li**[c,*]

[a]College of Biomedical Engineering & Instrument Science, Zhejiang University, Hangzhou 310027, China

[b]Department of Internal Medicine, University of California Davis, Sacramento, CA 95817, USA

[c]Department of Biochemistry and Molecular Medicine, UC Davis Comprehensive Cancer Center, University of California Davis, Sacramento, CA 95817, USA

[d]Institute of Animal Husbandry and Veterinary Science, Zhejiang Academy of Agricultural Sciences, Hangzhou, Zhejiang 310021, China

[#] These authors contributed equally to this work.

Abstract

Compared to conventional carrier-assistant drug delivery systems (DDSs), drug self-delivery systems (DSDSs) have advantages of unprecedented drug loading capacity, minimized carrier-related toxicity and ease of preparation. However, the colloidal stability and blood circulation time of DSDSs still need to be improved. Here we report on the development of a novel biomimicry drug self-delivery system by the integration of a top-down cell membrane complexing technique into our self-delivery multifunctional nano-platform made from bottom-up approach that contains 100% active pharmaceutical ingredients (API) of Pheophorbide A and Irinotecan conjugates (named PI). Compared to conventional cell membrane coated nanoparticles with polymer framework as core and relatively low drug loading, this system consisting of red blood cell membrane vesicles complexed PI (RBC-PI) is polymer-free with up to 50% API loading. RBC-PI exhibited 10 times higher area under curve in pharmacokinetic study and much lower macrophage uptake compared with the parent PI nanoparticles. RBC-PI retained the excellent chemophototherapeutic effects of the PI nanoparticles, but possessed superior anti-cancer efficacy with prolonged blood circulation, improved tumor delivery, and enhanced photothermal effects in animal models. This system represents a novel example of using cell membrane complexing technique for effective surface modification of DSDSs. This is also an innovative study to form a polymer-free cell membrane nanoparticle complexing with positive surface charged materials.

* lypli@ucdavis.edu; tylin@ucdavis.edu.

Author Contributions

X.B.X, Y.P.L, T-Y.L, X.D.X, G.M.Y and J.K.T conceived the study and wrote the paper; The in vitro and in vivo study was by X.B.X; Cyo-TEM were support by H.E.L, H.W. D.J, Y.E.H, W.Y, C-X.P and W.W.X provided Animal experiment support; All authors reviewed and approved the manuscript.

Conflicts of interest

All authors declare no conflict of interest.

This biomimicry DSDS takes advantages of the best features from both systems to make up for each other's shortcomings and posed all the critical features for an ideal drug delivery system.

Abstract

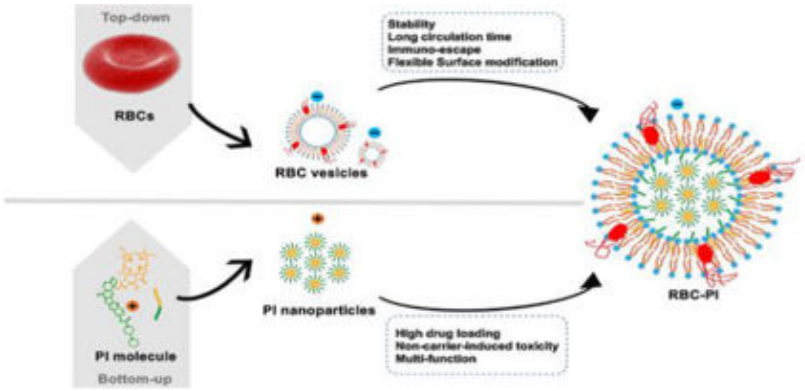

The pure drug self-delivery system with cell membrane modified to create a unique class of ideal drug delivery platform

Introduction

Chemotherapy has been one of the major clinic treatment approaches for cancers in the past few decades[1]. However, the unbearable toxicity and unfavourable pharmacokinetics (PK) of chemotherapeutic agents greatly limit their clinical applications and affect the quality of life of patients. Nanocarrier-based drug delivery systems (DDSs) represent one of the promising approaches for addressing these issues. The ideal DDSs demand an improved performance over the whole aspects of stability, loading capacity, long half-life in blood for enhanced penetration and retention (EPR) effect, low carrier-related toxicity, multi-functionality, and controlled drug release ability, to achieve the best therapeutic index and toxicity profiles[2–4]. The drug self-delivery systems (DSDSs) have been an emerging paradigm, which could potentially achieve 100% drug loading, minimize carrier associated toxicity and enhance the drug delivery for an improved anti-cancer performance[5,6]. DSDSs could be achieved by the self-assembly of amphiphilic pro-drugs or pure drugs (including free drugs or drug-drug conjugates) into nanostructures[7]. The examples include carbamate-linked SN-38 self-assembled nanofibers[8], or nanoparticles co-assembled from physical mixtures of different free drugs, such as doxorubicin / 10-hydroxycamptothecin[9], doxorubicin / camptothecin[10]. However, DSDSs still suffer from short blood circulation time, ostwald ripening and colloidal instability[11]. The rapid clearance by the mononuclear phagocytic system lead to reduced efficacy and increased toxicity to normal organs[12]. Several approaches for surface modification of DSDSs had been proposed to achieve better stability and prolonged circulation half-life allowing more effective EPR effect and better therapeutic index. For example, poly(ethylene glycol) (PEG) had been broadly utilized to modify nanoparticles for enhanced biostability and water dispersibility[13, 14]. However, accelerated blood clearance due to newly developed anti-PEG immune responses after repeated dosing had been

hindering the clinical applications[13,15, 16]. Therefore, there is an unmet need to have a more biocompatible strategy to improve the efficacy & toxicity profiles of DSDSs.

The cell membrane-coating nanoparticles represent a pioneer top-down technology for creating biomimicry platforms to realize high biocompatibility, and thus effectively prolong the circulation time of payloads[17–24]. The typical structure of such nanoparticles consists of a nanoparticulate core (ex. poly(lactic-co-glycolic acid) (PLGA)[25,28] or Au nanopaticle[29] for drug loading and an outer layer of cell membrane derived from red blood cell (RBC)[30, 31], platelets, leukocytes, stem cells[32], or cancer cell[17]. RBC membrane is relatively easy to obtain and expressing surface CD47 as “don’t eat me” signal resulting in great reduction in macrophage engulfment[33]. Studies also revealed that compared to 15.8 hours for comparable PEGylated nanoparticles, RBC membrane coated nanoparticles could achieve a significantly longer elimination half-life of 39.6 hours without induction of cellular or humeral immune response after repeated administration. Unfortunately, the relatively low drug loading ratio (around 10%-20%)[34] due to the requirement of additional drug loading cores (e.g. PLGA) set a major hurdle for its future clinical translation[35]. Moreover, this cell membrane-coating technology has not been successfully applied in positive surface charge inner core thus far due to unexpected aggregation[36].

We recently developed a new type of self-indicating and self-delivery fully active pharmaceutical ingredients nanoparticles (FAPIN) based on the drug-photosensitizer conjugates (named PI) consisting of Pheophorbide A (Pa) and Irinotecan (Ir) through an ester bond[37]. We demonstrated that PI mediated light treatment not only produced heat and reactive oxygen species(ROS) but also triggered the release of chemotherapeutic drug at the tumor sites, resulting in synergistic anticancer effects *in vivo.* However, their relatively low stability and positive surface charge resulted in rapid systemic clearance and limited the future application. Furthermore, the lack of surface function groups caused difficulties for surface modification. Herein, we introduced a synergistically combined bottom-up and top-down strategy to complex cell membrane with our FAPIN to generate a new biomimicry DSDS without polymer core. With our newly established methods, cell membrane could then complex with strong positive charged materials to form novel nanostructures. Benefiting from this special architecture, we achieved several unique features: i) RBC membrane outer component provided immune evasion, decreased the strong positive surface charged, stabilized nanoparticle, and successfully prolonged the area under curve (AUC) by 10 times; ii) without a large percentage of polymer core, the cargo loading ratio achieved as high as 50% (RBC-PI (1:1)), eliminating the risk for the potential toxicity from additional core materials; iii) the light-responsive chemophototherapy could effectively eradicate lung cancers in animal models with improved drug delivery efficacy.

Experimental

Materials

Pheophorbide A (Pa) was bought from Santa Cruz Biotechnology. Irinotecan (Ir) was purchased from BIOTANG Inc. (MA, USA). 2’,7’-dichlorofluorescin diacetate (DCF-DA) and all solvents were purchased from Sigma-Aldrich (MO, USA).

Preparation of RBC-membrane-derived vesicles

An expired unit of donor packed red blood cells was acquired from the UC Davis Medical Center hospital transfusion services, and the provision approved by the Department of Pathology Clinical Research Oversight Committee Internal Review. RBC membrane was prepared according to previous studies with modification[16, 34]. Briefly, the RBCs were lysed in the hypotonic medium (0.25×PBS) for 90 mins on ice. Samples were centrifuged at 80000 × g for 90 min with a Beckman L7-65 Ultracentrifuge. The supernatant was removed and the pink pellet was re-suspended in water. The membrane protein concentrations were quantified using BCA protein assay kit (Pierce, Rock-ford, IL).

Synthesis and characterizations of RBC-PI nanoparticles

Synthesis of Pa and Ir conjugate (PI) was performed through ester formation according to our previous studies[37]. To synthesize RBC complexed PI (RBC-PI) nanoparticles, the PI conjugates were first dissolved in acetone at a 1 mg/mL concentration. One mL of the solution was added rapidly to 3 mL of water followed by adding 20 μL trimethylamine. The mixture was immediately put under Ultrasonic Cleaner (VEVOR, 110 W, 60 kHz) and homogenized for 30s at amplitude of 20%. After adding 1, 2, or 4 mg RBC cell membrane (calculated based on protein concentrations) to form RBC-PI with ratios of RBC membrane to PI at 1:1, 2:1, and 4:1; the solution was further sonicated in the water bath of a Digital Ultrasonic Cleaner (Vevor, 120 W, 40 kHz) for 2 minutes to form nanoparticles. After acetone and trimethylamine were removed by vacuum volatilization at room temperature.

The morphology of RBC-PI was observed under cryo-transmission electron microscopy (JEM-2100F, Tokyo, Japan), while the size distribution and zeta potentials were measured by dynamic light scattering (DLS) instrument (Zetasizer, Nano ZS, Malvern, UK). The stability test was performed in the presence of 10% FBS/PBS at the 1 mg/mL (PI concentration). The size distribution and polydispersity index (PDI) of each time point were tested by dynamic light scattering for a 30-day period.

Protein characterization of RBCs, RBC vesicles, RBC-PI and PI NPs was conducted using sodium dodecyl sulfate-polyacrylamide gel electrophoresis (SDS-PAGE) method reported in literature[33, 38]. Briefly, the samples in lithium dodecyl sulfate (LDS) loading buffer (Invitrogen) were heated to 90 °C for 10 min, and then 80 μg of sample was loaded into each well of a gel. The samples were run at 150 V for 1 h, and the resulting gel was stained in SimplyBlue (Invitrogen) overnight for visualization. To further explore the orientation of RBC membrane proteins, RBC-PI were incubated with 50 μg/mL trypsin for 1, 2, and 4 hours. Particle size and surface charge were measured with DLS at different time points.

Evaluation of *in vitro* ROS and heat production upon illumination

Different concentrations of RBC-PI or PI NPs were placed in 96-well plate, and exposed under 680 nm laser at 0.8 W/cm^2 (Shanghai, China) for 3 min. The heat generations were recorded by NIR thermal camera (FLIR, Santa Barbara, CA). The ROS productions were measured by using DCF-DA, as the indicator. Briefly, different concentrations of RBC-PI or PI NPs were incubated with 50 μM DCF-DA the working solution followed by light

treatment (680 nm, 0.8 W/cm^2 for 3 min). The fluorescence was quantified by SpectraMax M3 microplate reader (Molecular Devices, LLC, CA)

Drug release studies

Three hundred microliters of 50 μM RBC-PI (1:1) solutions adjusted to two different pH values (7.4 or 5.4) were placed in a 96-well plate. Each group at different pH was then treated with 0, 0.4, or 0.8 W 680 laser for 3 minutes. Laser was applied with 12 minutes interval to minimize the heat effect for drug release. At each time point, 2 μL of solutions from each sample were diluted into 98 μL DMSO to test released Ir fluorescence after light trigger. Of note, Ir fluorescence was quenched when conjugated with Pa[37].

Cell uptake and intracellular ROS production

The A549 cells were seeded in 96-well plates (1×10^4 cells/well) and incubated with RBC-PI and PI nanoparticles (PI: 25 μM). After 1, 2, 4, 6 and 8 hrs, the cells were lyzed with 0.5% Triton X-100 for 12 min and 4 times DMSO (v/v) were added. To quantify the particle uptake by A549 cells, fluorescence of PI were detected and normalized to the fluorescence at initial concentration (at 25 μM).

The A549 lung cancer cells were seeded in a 12-well dish (2×10^5 cells/well) and then incubated with 25 μM RBC-PI or PI NPs for 6 hours. After three times of washes with PBS, cells were incubated with 50 μM DCF-DA for 30 minutes. Samples were treated with or without light (630 nm, Omnilux New-U LED panel) for 1 minute, and intracellular PI uptake (based on Pa fluorescence) and ROS production were analyzed by flow cytometry (FACS Canton™, BD Bioscience, SD, CA).

Cellular uptake

The A549 lung cancer cells were seeded in glass-bottom dishes (Cellvis, Mountain View, CA) and treated with 25 μM RBC-PI. Two hours later, samples were replaced with fresh medium and treated with or without 630 nm LED light for 30 seconds every 2 hours. A relatively low light dose was used to avoid too much cytotoxicity. The intracellular fluorescence of Pa and Ir was monitored by fluorescence microscopy (Olympus IX81/IX2-UCB system, CV, PA) at different time points.

Cytotoxicity assay

Cell viabilities were determined by MTS method according to manufactory manual (Promega, Madison, Wl). A549 cells were seeded in 96-wells plates with a density of 5000 cells per well. The cells were treated with different concentrations of RBC-PI (1:1), PI NPs, free Pa and Ir at the comparable concentrations. Six hours later, medium was replaced with fresh complete media followed by illumination with 630 nm light for 3 minutes. After additional 24 hours incubation, MTS working solution was added and the absorbance at 490 nm was evaluated by Spectra Max M3 microplate reader. Experiments were performed in triplicate, and 3 independent experiments were conducted.

Cellular uptake study with macrophage-like cells

Human U937 macrophage-like cells were seeded in 96-well plates at a density of 5000 cells per well overnight. U937 cells were stimulated with 10 nM of phorbol 12-myristate 13-acetate (PMA) (Sigma-Aldrich) for 24 hours. Samples were replaced with fresh medium and treated with RBC-PI (1:1) and PI NPs at the concentration of PI molecule at 25 μM. The cells were then incubated with 0.5% Triton X-100 for 12 min and then added into 4 times DMSO (v/v). To quantify the particle uptake by U937 cells, fluorescence of Pa was detected by using an SpectraMax M3 micro-plate reader.

Pharmacokinetic evaluation

All animal studies were approved by the University of California Davis Institutional Animal Care and Use Committee (IACUC # 07-13119 and 09-15584) and the procedures were in accordance with institutional guidelines. The jugular vein cannulated female Sprague–Dawley rats (200g) were purchased from Harland (Indianapolis, IN) allowing easy drug administration and multiple blood collections. Five mg/kg RBC-PI (1:1) and PI NPs (2.5 mg/kg of Pa and 2.5 mg/kg of Ir) were i.v. administrated into rat (n = 3 for each group). Whole blood samples (~150 μL) were collected via jugular vein catheter at the predetermined time points post injection. Twenty microliters of plasma samples were mixed with 80 μL DMSO and Pa fluorescence was measured using Ex/Em: 412/680 nm channel. Untreated plasma was served as a blank control. The fluorescence spectra and standard curve were shown in Figure S1.

Anti-cancer efficacy study in tumor bearing mice

4-6 weeks of nude mice were purchased from the Jackson Laboratory (Sacramento, CA). Lung cancer bearing models were established by subcutaneously injecting $2\times l0^6$ A549 cells into flank. After tumor reaching the size of 500-650 mm^3, mice were than randomly assigned into 4 groups: PBS, free mixture of Pa and Ir, PI NPs and RBC-PI (1:1) (equal to 10 mg/kg of Pa and 10 mg/kg of Ir) (n=6 per group). Drugs were intravenous (i.v.) injected and tumors were illuminated at 24 h, 48 h, 72 h and 96 hours post-injection. The whole tumor region was covered by the light spot (0.8 cm^2 in diameter) generated from a 680 nm laser with 1.2 W/cm^2 for 3 min. Tumor surface temperature was determined by a NIR thermal camera. Animals were monitored every day, and body weight and tumor size were measured twice a week. The tumor size was calculated using the following formulation: Length × $Width^2/2$ (mm^3).

In vivo bio-distribution study

The *in vivo* biodistribution study was evaluated in the A549 tumor bearing mice. After tumor reached 500-650 mm^3 in size, tumor-bearing mice were randomly assigned into two groups (n=3 per group): RBC-PI (1:1) and PI NPs (20 mg/kg PI, equal to 10 mg/kg of Pa and 10 mg/kg of Ir). Forty-eight hours post i.v. injection, mice were sacrificed, and tumors and major organs were collected. About 100 mg of each organ were homogenized in PBS, followed by centrifugation at 20,000 × g for 10 min. The collected supernatants were added 5 times methanol to precipitate the protein. The solvent was further removed by vacuum. The PI (based on Pa fluorescence) concentration was measured by redissolution in methanol

with Spectra Max M3 microplate reader. Results were expressed as PI weight in per gram of tissue and normalized to the total dose of i.v. injection. The fluorescence spectra and standard curve were shown in Figure S1.

Statistical analysis

Data are presented as mean ± standard deviation (SD). Group comparisons were carried out using one-way analysis of variance or Student's *t* test. *P* value less than 0.05 was considered statistically significant difference.

Results and discussion

Preparation and Characterization of biomimicry RBC-PI complex

We previously developed a novel full-API nanoparticle (PI) self-assembled from the conjugates of a hydrophobic photosensitizer, pheophorbide A (Pa), and Irinotecan (Ir), a relatively hydrophilic anti-neoplastic drug. Based on its amphipathic nature, PI could self-assemble into nanoparticles without excipients, and could be used for tri-model treatment modalities, including photodynamic therapy, photothermal therapy and chemotherapy[37]. However, PI NPs were not very stable and their strong positive charge (+42 mV) resulting in less-ideal blood circulation time (9.1± 2.7 h), and thus rendered their full potentials for cancer therapy. Inspired by the interesting strategy of using RBC cell membrane biomimicry surface modification to dramatically extend nanoparticle's circulation time, we first introduced cell membrane to modify PI NPs based drug self-delivery system to improve their stability, PK profile and anti-therapeutic index.

Firstly, RBC cell membrane was extracted by hypotonic shock followed by mini-extrusion (Scheme 1 and Figure 1a). At the initial intend, with simple mixing strategy, strongly positively charged PI NPs rapidly interacted with negatively charged RBC vesicles resulting in precipitation through strong electrostatic force. This was similar with the finding described by Luk et al when they tried to mix RBC vesicles with positively charged PLGA polymeric cores[36]. It is interesting to note that most reported cell membrane coated nanoparticles required a core which usually had the negative zeta potential, as this would allow cell membrane to coat on the surface through extrusion or self-assemble[17–19]. One exception was silica/silicon nanoparticles which had weak positive charge (+5 - +15); however, based on the published TEM pictures cell membrane formed "small aggregates" on the silica surface[39–41].

To circumvent this limitation, we newly developed a method using triethylamine (TEA) to temporarily neutralize the positive charge of PI NPs to prevent the strong electrostatic interaction and aggregation[36](Figure S2). Under this condition, RBC membrane was then added and TEA was slowly removed followed by a short 2-minute sonication. This method allowed RBC vesicles and PI NPs to form stable nanoparticles.

To further characterize this new nanostructure formed by PI and RBC membrane, we used different ratios of these two components and evaluated the changes in size, zeta potential, and morphology. As seen in the Figure 1 a, b and Figure S3, the RBC vesicles and PI NPs exhibited an average diameter of 190 nm and 50 nm with zeta potential of −31 mV and +43

mV, respectively. When we assembled them together with different ratios using the method described above, nanoparticles could be formed with the ratios of 1:1 to 4:1 (RBC vesicles protein concentration to PI molecular weight ratio), but not 0.5:1 due to its undesirable size and stability (Figure S4). The size of the resulting RBC-PI fell between the original PI NPs and vesicles formed by cell membrane; and this was RBC vesicles amount-dependent (Figure 1a, b). Also, the zeta potential of the nanoparticles with different ratios also decreased from +43 mV to −29 – −32 mV, which was comparable with that of the RBC membrane vesicles (Figure 1d). Those results indicated that the surface of PI nanoparticles was successfully modified by the RBC vesicles.

However, the membrane amount-dependent size changes were unexpected as the sizes of other types of cell membrane coated core-shell nanoparticles were solely based on the core size[36]. Therefore, we suspected the formation of a distinct structure and the occurrence of additional interactions between RBC membrane and PI monomers. Cryo-electron microscopy was employed to visualize the morphology changes of RBC-PI nanoparticles at different ratios (Figure 1c, d). A “core-like” structure was observed with a membrane amount-dependent increase in size, but the density of “core-like” structures decreased. When the ratio of RBC protein concentration to PI was set to 4:1, excess cell membrane stretch from the “core-like” nanoparticles to form a “hand-bag” structure (Figure 1d).

In our system, we believe that the weak intermolecular forces between RBC membrane and PI resulted in stable RBC-PI nanoparticles. Solid particles in a liquid medium are subject to weak interaction forces. Among those forces, van der Waals forces, hydrogen bonds and π-π interactions are the most important low-energy forces in self-assembled systems for keep nanoparticles stable[42, 43]. These forces combined both attractive and repulsive interactions which depend on aggregation degree of intermolecular[44]. These phenomena could be exactly observed in our cyro-EM images (Figure 1c, d). We speculated that PI monomers dispersed in both aqueous core and bilayer of RBC vesicles. When the ratio of RBC protein concentration to PI close to 1:1, attraction was the dominant force to keep RBC-PI nanoparticles stable in a comparative small size (around 60 nm). These attraction interactions come from both PI to PI and PI to glycoproteins and sialic acid of RBC vesicles. In addition, Luk[19, 36] and co-author studied on the interfacial interactions between natural RBC membranes and synthetic polymeric nanoparticles and in their study repulsive force of glycoprotein and sialic acid is important to their nanoparticles formation. In the end, along with increasing amounts of RBC vesicles, repulsive force made nanoparticles bigger and finally part of RBC membrane stretched outside (Figure 1d).

These unique morphological and structural features distinguished RBC-PI nanoparticles from other reported cell membrane coating core-shell nanoparticles[25, 28] or liposome-like drug loading nanoparticles[29]. The reported cell membrane coating core-shell nanoparticles usually had a firm polymeric core on which membrane could be attached through the electrostatic interaction and hydrophobic force. Additionally, the negative surface charged cores played an important role in the formation of membrane coating core-shell nanoparticles while the positively charged cores formed observable aggregates because of the strong electrostatic interaction[36, 45]. Zhang et al[38] reported a cell membrane-cloaked chemotherapy drug doxorubicin and photothermal/photodynamic drug indocyanine green

self-assembling nanoparticle. Compared to this kind of formulation, our RBC-PI did not form like a membrane coating core-shell structure, which were more like PI molecule and RBC self-assembling. Our formulation also differs from liposome formulations, which usually load hydrophobic drugs inside their phospholipid bilayer or hydrophilic drug into their aqueous core. Their ring-shaped phospholipid bilayer structures and discrete structures of drug could easily be recognized in cryo-EM images due to the comparatively high contrast of the liposomes and drug precipitates[46, 47]. However, a typical double-layered structure was not observed on the nanoparticle surface (Figure 1c), these may also be attributed to PI molecules distributed in both aqueous core and bilayer of RBC vesicles that decreased the contrast between the bilayer and core[24, 27]or liposome-like drug loading nanoparticles[28]. In the end, these results suggested that RBC membrane not only modified the particle surface, but also complexed with PI to jointly form the “core-like” structure (Figure 1b).

To characterize the pattern of RBC-PI, we performed SDS-PAGE experiments and showed that RBC-PI nanocomplex still maintained the protein pattern similar to that of normal RBCs (Figure 1e). Next, we intend to explore the orientation of the RBC membrane proteins, we trypsinized the glycoproteins on the surface of RBC membrane. RBC-PI were incubated with 50 μg/mL trypsin. 1, 2 and 4 hours following the trypsinization, the changes of particle size and zeta potentials were monitored. Since RBC bilayer membranes are impermeable to trypsin[48]. The trypsinization could only digest those right-side-out membrane proteins. As shown in the Figure 1f, at 2 hour time point, surface negative charges were lost and the size of RBC-PI slightly increased. At 4 hours, large aggregates were formed and these results suggested that surface glycoproteins that were responsible for membrane structure stabilization be digested by trypsin resulting instability. However, because of we did not confirm the results by using the anti-body of surface makers such as CD47 and CD59, the orientation of the RBC membrane proteins still need to be further investigated.

Physical and functional analysis of RBC-PI

The PI NPs and RBC-PI nanoparticles showed similar UV spectra with characteristic peaks at 370 nm, which represented the characteristic absorption of Ir. The characteristic absorption of Pa were shown at 412 and 670 nm. However, the 412 nm peak overlapped with 370 nm peak of Ir (Figure 2a). Similar to other RBC-coating nanoparticles[49], we observed a red-shift of about 20 nm from 400 to 420 nm along with increased **RBC** membrane to **PI** ratio.

To further dissect the unique architecture of our nanoparticles, we performed further experiments to compare the changes in physical and functional properties of RBC-PI at different RBC vesicles-to-PI ratios. As an intrinsic photosensitizer, PI NPs could produce fluorescence, heat and ROS for image-guided cancer therapy[37]. Due to the π-π interaction, the fluorescence of PI NPs was quenched in water but could be recovered after dissociation in 10% SDS solution (Figure 2 b-c). We hypothesize that the package of PI molecules in RBC-PI after interaction with cell membrane was less compact compared to that in the parent PI NPs resulting in less quenching effects. Interestingly, with the increasing RBC

vesicles-to-PI ratios, the degree of fluorescence quenching diminished in water (Figure 2b). The fluorescence of all nanoparticles dramatically increased after dissociation in the presence of 10% SDS (Figure 2b). The quenching ratio (fluorescence in the present of SDS/ fluorescence in water) decreased from 140 to 55 for PI NPs (0:1) to RBC-PI (4:1) with increasing amount of cell membrane. Similarly, there was a dose-dependent ROS production for both PI NPs and RBC-PI. RBC-PI (4:1) had the highest ROS production which was in line with its lowest quench effects. Interestingly, this ROS production could be also partially contributed by the components of RBC membrane, as RBC vesicles also produced ROS upon illumination (Figure 2d).

Lastly, a dose-dependent temperature increase in both PI NPs and RBC-PI nanoparticles upon illumination were also observed (Figure 2e). When the PI molecules self-assembled and quenched, it could induce a structural reconfiguration and the most photo-energy was transformed into heat depending on the ratio of quenching[50]. Therefore, when quenching ratio in molecular motion decreased with the increased amounts of cell membrane (Figure 2b, c), the heat production ability decreased (Figure 2e). Intriguingly, similar to ROS production, RBC membrane vesicle appeared to play a role in heat production in RBC-PI. Thus, at the similar quenching ratio between PI NPs and RBC-PI (1:1). In additionally, RBC-PI (1:1) had significant higher heat production (Figure 2e). These phenomena could be likely attributed to the RBC intrinsic hemoglobin bound protoporphyrin and iron[51–53]. The presence of protein in RBC membrane was detected in the SDS-PAGE of red blood cells and RBC membrane (Figure 1e). Collectively, these results strongly supported our notion that RBC membrane endowed into PI NPs resulting in physical and functional changes, but not a simple surface coating like other reported cell membrane coating core-shell nanoparticles.

The nanostructures of PI suffered from ion change in different solutions resulting in aggregation. The small size of pure nanodrug have massive surface area results in sufficiently high free energy or surface charge that might cause attraction or agglomeration[54], which leads to recrystallization into larger particles. This also known as ostwald ripening[11]. Furthermore, pure nanodrug that consists of water-insoluble drugs are always susceptible to precipitation upon dilution in blood, gastric and other body fluids after administration into the body[55, 56]. Therefore, excipients or stabilizer are still needed in pure drug self-delivery systems. We investigated the stability of RBC-PI in PBS (pH 7.4) solution the presence of fetal bovine serum (FBS). As shown in Figure 2f, RBC-PI displayed excellent stability through a 30 days period in terms of size and PDI. We also test the stability of RBC-PI in presence of 100% FBS and homologous human serum. Despite an initial increase, the particle size of RBC-PI in these biological media were stable at least 7 days (Figure S5 a&b). In contrast, PI NPs were not stable for long-time (Figure S5 c&d) and precipitated within 7 days in the presence of FBS. Based on this, the new cell membrane complexing technique described here provides a perfect solution to enhance the *in vivo* stability of these pure drug self-delivery systems.

In vitro light triggered chemophototherapy of RBC-PI

Since RBC-PI (1:1) was very stable even in the presence of serum, and had the highest drug loading ratio and the smallest size for potentially better tissue penetration, we chose this

formulation for the following *in vitro* and *in vivo* studies. Tumor cell uptake of PI and RBC-PI were compared at different time points. We found that tumor cells had significantly faster uptake of PI comparing to RBC-PI at 2 and 4 hours (Figure 3a) presumably due to their strong positive surface charge. However, there were no difference with longer incubation time (6 & 8 hours), as both PI and RBC-PI reached saturation. Similar amount of cellular uptake at 6 hours were also confirmed with flow cytometry (Figure S6). Interestingly, with similar degree of uptake, upon laser illumination, RBC-PI treated cells had higher intracellular ROS production compared to PI NPs treated cells (Figure 3b), which was consistent with the finding that RBC-PI had better ROS production efficiency (Figure 2d), compared to PI NPs. Cells treated with free irinotecan did not produce intracellular ROS upon light treatment (Figure S7).

Pa and Ir was conjugated with an ester bond, which could be cleaved in the presence of acidic pH (e.g. pH 5.4 in the lysosome) resulting in drug release. Similar to our previous finding in PI NPs[37], Ir release triggered by light displayed significant higher efficiency in the acidic pH than neutral pH at a high light dose (Figure 3c). The drug release kinetics could be also monitored at the cell line level under a fluorescence microscope. A549 cells were treated with RBC-PI followed with laser treatments or without laser treatments. Figure 3d illustrated a time-dependent RBC-PI uptake evidenced by increased porphyrin signals, which came from the free Pa molecules cleaved from PI conjugates inside cells after the dissociation of RBC-PI. The blue fluorescence Ir was quenched when conjugated with Pa, but was restored after cleavage from PI conjugates upon light treatment. In contrast, without light treatment, lower level of both Pa and Ir signals was appreciated indicating a slower drug release process without light treatment, as the uptake amount should be the same. Those results confirmed that similar to PI NPs[37], laser could also markedly expedite the drug release from RBC-PI.

Pharmacokinetics and macrophage uptake

As shown in Figure 2f, we have demonstrated that RBC-PI displayed excellent stability throughout the 30-day period with minimal changes in both size and PDI. The rapid clearance of nanoparticles from the blood because of the recognition by immune system undoubtedly limits the time window for their passive tumor accumulation via EPR effect[57–59]. In addition, a strong positive charge surface also enhanced macrophage uptake[60]. PI nanoparticles suffered from low serum stability and rapid clearance partially due to strong positive charges, while RBC-PI nanocomplex should greatly overcome those drawbacks. As expected, we demonstrated that RBC-PI had superior pharmacokinetic profile to PI NPs in rats. As seen in the Figure 4a and Table S1, RBC-PI had significant longer half-life (17.3 vs 9.1 h) and almost 10 times higher area under curve (AUC) (58824 vs 5902.7 ug/L*h) than PI NPs.

In addition to the attribute from the enhanced serum stability, we believed RBC membrane modification further decreased macrophage uptake resulting in slower clearance. Therefore, we incubated RBC-PI and PI with PMA activated human U937 macrophage-like cell lines for 2, 4, and 8 hours. The macrophage phagocytosis of RBC-PI and PI were quantified based on fluorescence intensity of Pa. There was a time-dependent macrophage uptake of PI NPs

(Figure 4b). At 8 hours, RBC-PI had more than 8 times less macrophage uptake compared to PI. Similar results were observed using mouse macrophage-like cell line RAW 264.7 (Figure S8), but in less difference (2 times less uptake). RBC-PI appeared to be recognized by mouse macrophages. This could be because mouse macrophages could still recognize the species difference on human RBC surface antigens. This was fully expected, while other studies usually employed rodent RBCs for their study[22] and thus did not encounter these phenomena.

In our system PI NPs were improved the biocompatibility by RBC membrane. Functional RBC cell membrane proteins such as CD47 and CD59 have been identified on RBC surfaces as self-markers that actively signal macrophages and prevent their uptake[61, 64]. Those inherited surface markers could protect cell membrane coated nanoparticles from immune surveillance[59, 60]. Therefore, the immune-evasive function of RBC-PI was attributed by two factors: i) compared to strong positive charge of PI NPs, the negative surface charge of RBC-PI were less preferred for phagocytosis by macrophage cells; ii) the “don’t eat me” surface markers inherited from RBCs on the RBC-PI surface could prevent macrophage uptake.

One may challenge that the PK of RBC-PI was still far shorter than that of RBCs. To maximize the benefit of RBCs, RBC-hitchhiking approach was utilized to bound nanoparticle to live circulating RBCs allowing remarkably prolonged blood circulation times *in vivo*[65–68]. These surface coupling strategies avoided damaging encapsulation procedures and therefore offer theoretical advantages of drug loading without compromising RBC biocompatibility[69]. With the RBC-hitchhiking approach, the circulation time is associated with RBC (naturally exists in the body), but for the RBC membrane coating strategy such as RBC-PI, the circulation time is more associated with the original nanoparticles (foreign body). Furthermore, in contrast to the much larger size of RBC (~8 μm in diameter), the size of RBC-PI was in nanometer range (around 100 nm). The size related effects on circulation/elimination kinetics are also different. Therefore, it is not surprising that the circulation time of RBC membrane coated nanoparticles is shorter than the life-span of RBCs (or RBC-hitchhiked materials). However, the particle size also had great impact on nanoparticles margination in blood vessels and the way of diffusion in tissues[30, 70, 71]. The smaller size of RBC membrane coated nanoparticles may offer better opportunity to take advantage of the leaky tumor blood vessels for tumor-targeted drug delivery. In this research, we showed the benefit of complexing limited amount RBC membrane to improve the biocompatibility of PI nanoparticles and tumor-targeted drug delivery while keeping the relatively high API loading (50%) of the final nanocomplex.

In vitro chemophototherapeutic effects

The *in vitro* cytotoxic effects of the free drug, PI NPs and RBC-PI were evaluated in A549 cells. Free drug, PI NPs and RBC-PI were all exhibited negligible cytotoxicity without light treatment which indicated that RBC membrane did not cause toxicity and the Ir release was limited such condition (Figure 5a-b). In contrast, upon light treatment, a dose-dependent antitumor activity was observed in free Pa, PI NPs and RBC-PI groups. The IC_{50} values for

PI NPs, Pa and RBC-PI are 12.7, 7.0 and 5.4 μM, respectively. The above results indicated that RBC-PI retained the chemophototherapeutic effect of PI NPs.

In vivo antitumor efficacy

To assess the *in vivo* antitumor efficacy, the A549 tumor-bearing mice were administrated with free Pa + Ir, PI NPs and RBC-PI on day 1, 7 and 21; tumors were treated with laser (680 nm, 1.2 W/cm^2) for 3 min at 24, 48, 72, and 96 hours post-injection. As shown in Figure 5c and Figure S9, free Pa+Ir and PI NPs treated groups showed better tumor reduction than PBS control. Among all treatment groups, RBC-PI group displayed the best anti-tumor efficacy. The body weight of the mice showed negligible variation during the treatment (Figure 5d) suggesting a generally low toxicity in all groups.

Local heat production is one of the major factors to destroy local tumor for PI mediated phototherapy[37], and thus we recorded the tumor surface temperature at different time points post-injection (Figure 5e and Figure S10). Tumor surface temperature in Pa+Ir, PI NPs, and RBC-PI groups were all increased compared to that in PBS group. Among those days, 48 hour time point appeared to reach the peak for all treatment groups and temperature started to decline afterwards. Most importantly, RBC-PI treated groups had significantly higher tumor temperature increase than both PI NPs and Pa+Ir groups even after 96 hours. This was presumably due to the longer circulation time after RBC vesicles complexing allowing significantly better drug accumulation at the tumor sites, which was also confirmed with the biodistribution study (Figure 5f). Besides, this result was consistent with our prior findings that RBC-PI (1:1) had better heat production ability than PI NPs at the same concentration (Figure 2e). Unfortunately, we only observed a slight but not significant lower trend for the liver uptake in RBC-PI treated groups. As previously mentioned, this could be because mouse macrophages could still recognize human surface antigens due to species differences.

In addition to use the body weight changes for evaluation of systemic toxicity, we collected major organs for histopathology examination. There was minimal off-target toxicity detected in the organs examined (Figure Sll). Tumors collected from the free Pa+Ir, PI NPs, and RBC-PI mediated chemophototherapy were also assessed. Compared to the PBS control group, free Pa+Ir treated tumor had some degrees of cell separation, while PI NPs and RBC-PI groups showed obvious decrease in cell density. Nuclear condensations and fragmentations and loss of cell morphology all suggested ongoing apoptosis and necrosis progresses after treatment. Taken together, we demonstrated that RBC-PI had superior *in vivo* anti-cancer therapeutic efficacy with high biocompatibility and low systemic toxicity.

Conclusions

This study introduces the top-down cell membrane technology to modify drug self-delivery system made from bottom-up approach that could now achieve good storage & serum stability, prolonged circulation time and multi-treatment modalities without increased toxicity from the excipient. There are potentials to replace membranes from RBC with that from different types of cells (e.g. platelets, macrophages and stem cells) for additional functionalities. On the other hand, this paper also demonstrates a new method to form a biomimicry nanoparticle without polymer/nanoparticle cores and thus dramatically

circumvent the drug loading limitation and eliminate the risk from carrier core related toxicity. Our newly developed complexing methods further overcome the limitation of cell membrane coating technology on the core with positive surface charges. The complexed nanoparticles can achieve as high as 50% API loading (RBC-PI (1:1)) which is 2-5 folds higher than that other cell membrane coated nanoparticles[20]. The resulting biomimicry and multi-functional drug self-delivery system maintained the original strength of each system and perfectly made up each other's deficiency to form an almost perfect delivery system. This study created a great platform to design ideal biomimicry DSDSs for future clinical translation for cancer treatment and other biomedical applications. This nanofabrication via synergistic combination of bottom-up and top-down approaches may encourage researchers to create many new nano-systems with unique features to solve complicated biomedical problems.

Supplementary Material

Refer to Web version on PubMed Central for supplementary material.

Acknowledgements

We thank Fei Guo, Ph.D. from biological electron microscopy core facility at UC Davis for his help with the Cryo-EM studies as well as the financial support from NIH/NCI (R01CA199668, R01CA232845 and R01CA176803), NIH/NICHD (R01HD086195), Veterans Affairs Merit Review (Award # 101 BX001784 and 1I01BX003840-01) and ACS IRG (95-125-13), and UC Davis Comprehensive Cancer Center Support Grant (CCSG) awarded by the National Cancer Institute (NCI P30CA093373). The contents do not represent the views of the U.S. Department of Veterans Affairs or the United States Government.

Notes and references

1. DeSantis CE, Lin CC, Mariotto AB, Siegel RL, Stein KD, Kramer JL, Alteri R, Robbins AS and Jemal A, C4; a cancer journal for clinicians, 2014, 64, 252–271.
2. Chen G, Qiu H, Prasad PN and Chen X, Chem Rev, 2014, 114, 5161–5214. [PubMed: 24605868]
3. Blanco E, Shen H and Ferrari M, Nature biotechnology, 2015, 33, 941.
4. Matsumura Y and Maeda H, Cancer Res, 1986, 46, 6387–6392. [PubMed: 2946403]
5. Qin S-Y, Zhang A-Q, Cheng S-X, Rong L and Zhang X-Z, Biomaterials, 2017, 112, 234–247. [PubMed: 27768976]
6. Zolnik BS, Gonzalez-Fernandez A, Sadrieh N and Dobrovolskaia MA, Endocrinology, 2010, 151, 458–465. [PubMed: 20016026]
7. Liu J, Huang W, Pang Y and Yan D, Chem Soc Rev, 2015, 44, 3942–3953. [PubMed: 26008957]
8. Kasai H, Murakami T, Ikuta Y, Koseki Y, Baba K, Oikawa H, Nakanishi H, Okada M, Shoji M and Ueda M, Angew Chem Int Ed, 2012, 51, 10315–10318.
9. Yu C, Zhou M, Zhang X, Wei W, Chen X and Zhang X, Nanoscale, 2015, 7, 5683–5690. [PubMed: 25740312]
10. Barua S and Mitragotri S, ACS nano, 2013, 7, 9558–9570. [PubMed: 24053162]
11. Huang P, Wang D, Su Y, Huang W, Zhou Y, Cui D, Zhu X and Yan D, J Am Chem Soc, 2014, 136, 11748–11756. [PubMed: 25078892]
12. Wang X, Wang X and Guo Z, Acc Chem Res, 2015, 48, 2622–2631. [PubMed: 26247558]
13. Dobrovolskaia MA, Aggarwal P, Hall JB and McNeil SE, Mol Pharm, 2008, 5, 487–495. [PubMed: 18510338]
14. Zhou M, Zhang X, Yang Y, Liu Z, Tian B, Jie J and Zhang X, Biomaterials, 2013, 34, 8960–8967. [PubMed: 23958027]

15. Ishida T, Wang X, Shimizu T, Nawata K and Kiwada H, J Control Release, 2007, 122, 349–355. [PubMed: 17610982]
16. Bartneck M, Keul HA, Zwadlo-Klarwasser G and Groll J. r., Nano Lett, 2009, 10, 59–63.
17. Fang RH, Hu CM, Luk BT, Gao W, Copp JA, Tai Y, O'Connor DE and Zhang L, Nano Lett, 2014, 14, 2181–2188. [PubMed: 24673373]
18. Gao W and Zhang L, J Drug Target, 2015, 23, 619–626. [PubMed: 26453159]
19. Luk BT and Zhang L, J Control Release, 2015, 220, 600–607. [PubMed: 26210440]
20. Hu C-MJ, Fang RH, Wang K-C, Luk BT, Thamphiwatana S, Dehaini D, Nguyen P, Angsantikul P, Wen CH, Kroll AV, Carpenter C, Ramesh M, Qu V, Patel SH, Zhu J, Shi W, Hofman FM, Chen TC, Gao W, Zhang K, Chien S and Zhang L, Nature, 2015, 526, 118. [PubMed: 26374997]
21. Dehaini D, Wei X, Fang RH, Masson S, Angsantikul P, Luk BT, Zhang Y, Ying M, Jiang Y, Kroll AV, Gao W and Zhang L, Adv Mater, 2017, 29, 1606209–1606217.
22. Chen W, Zeng K, Liu H, Ouyang J, Wang L, Liu Y, Wang H, Deng L and Liu YN, Adv Funct Mater, 2017, 27, 1605795–1605804.
23. Hu Q, Sun W, Qian C, Bomba HN, Xin H and Gu Z, Adv Mater, 2017, 29, 1605803–1605811.
24. Villa CH, Anselmo AC, Mitragotri S and Muzykantov V, Adv Drug Deliv Rev, 2016, 106, 88–103. [PubMed: 26941164]
25. Fu Q, Lv P, Chen Z, Ni D, Zhang L, Yue H, Yue Z, Wei W and Ma G, Nanoscale, 2015, 7, 4020–4030. [PubMed: 25653083]
26. Sun H, Su J, Meng Q, Yin Q, Chen L, Gu W, Zhang P, Zhang Z, Yu H and Wang S, Adv Mater, 2016, 28, 9581–9588. [PubMed: 27628433]
27. Copp JA, Fang RH, Luk BT, Hu C-MJ, Gao W, Zhang K and Zhang L, Proc Natl Acad Sci U S A, 2014, 111, 13481–13486. [PubMed: 25197051]
28. Wei X, Gao J, Fang RH, Luk BT, Kroll AV, Dehaini D, Zhou J, Kim HW, Gao W and Lu W, Biomaterials, 2016, 111, 116–123. [PubMed: 27728811]
29. Gao W, Hu CMJ, Fang RH, Luk BT, Su J and Zhang L, Adv Mater, 2013, 25, 3549–3553. [PubMed: 23712782]
30. Villa CH, Seghatchian J and Muzykantov V, Transfus Apher Sci, 2016, 55, 275–280. [PubMed: 27856317]
31. Muzykantov V, Expert Opin Drug Deliv, 2013, 10, 1–4. [PubMed: 23176316]
32. Toledano Furman NE, Lupu-Haber Y, Bronshtein T, Kaneti L, Letko N, Weinstein E, Baruch L and Machluf M, Nano Lett, 2013, 13, 3248–3255. [PubMed: 23786263]
33. Hu CM, Zhang L, Aryal S, Cheung C, Fang RH and Zhang L, Proc Natl Acad Sci U S A, 2011, 108, 10980–10985. [PubMed: 21690347]
34. Gupta N, Patel B and Ahsan F, Pharm Res, 2014, 31, 1553–1565. [PubMed: 24449438]
35. Dong X, Niu Y, Ding Y, Wang Y, Zhao J, Leng W and Qin L, Nanoscale Res Lett, 2017, 12, 202–215. [PubMed: 28314369]
36. Luk BT, Hu C-MJ, Fang RH, Dehaini D, Carpenter C, Gao W and Zhang L, Nanoscale, 2014, 6, 2730–2737. [PubMed: 24463706]
37. Xue X, Huang Y, Wang X, Wang Z, Carney RP, Li X, Yuan Y, He Y, Lin T.-y. and Li Y, Biomaterials, 2018, 161, 203–215. [PubMed: 29421556]
38. Zhang N, Li M, Sun X, Jia H and Liu W, Biomaterials, 2018, 159, 25–36. [PubMed: 29309991]
39. Parodi A, Quattrocchi N, Van De Ven AL, Chiappini C, Evangelopoulos M, Martinez JO, Brown BS, Khaled SZ, Yazdi IK, Enzo MV, Isenhart L, Ferrari M and Tasciotti E, Nat Nanotechnol, 2013, 8, 61–68. [PubMed: 23241654]
40. Palomba R, Parodi A, Evangelopoulos M, Acciardo S, Corbo C, De Rosa E, Yazdi I, Scaria S, Molinaro R and Furman NT, Sci Rep, 2016, 6, 34422. [PubMed: 27703233]
41. Su J, Sun H, Meng Q, Zhang P, Yin Q and Li Y, Theranostics, 2017, 7, 523–537. [PubMed: 28255347]
42. Boström M, Williams D and Ninham B, Phys Rev Lett, 2001, 87, 168103–168104. [PubMed: 11690249]

43. Whitesides GM and Boncheva M, Proc Natl Acad Sci U S A, 2002, 99, 4769–4774. [PubMed: 11959929]
44. Merisko-Liversidge E and Liversidge GG, Adv Drug Deliv Rev, 2011, 63, 427–440. [PubMed: 21223990]
45. Fondell A, Edwards K, Ickenstein LM, Sjöberg S, Carlsson J and Gedda L, Eur J Nucl Med Mol Imaging, 2010, 37, 114–123. [PubMed: 19662408]
46. Mornet S, Lambert O, Duguet E and Brisson A, Nano Lett, 2005, 5, 281–285. [PubMed: 15794611]
47. Semple SC, Leone R, Wang J, Leng EC, Klimuk SK, Eisenhardt ML, Yuan Z-N, Edwards K, Maurer N and Hope MJ, J Pharm Sci, 2005, 94, 1024–1038. [PubMed: 15793796]
48. Heidrich HG and Leutner G, Eur J Biochem, 1974, 41, 37–43. [PubMed: 4816455]
49. Pei Q, Hu X, Zheng X, Liu S, Li Y, Jing X and Xie Z, ACS nano, 2018, 12, 1630–1641. [PubMed: 29346736]
50. Dhotel A, Chen Z, Delbreilh L, Youssef B, Saiter J-M and Tan L, Int J Mol Sci, 2013, 14, 2303–2333. [PubMed: 23348927]
51. Sandberg S, Talstad I, Hovding G and Bjelland N, Blood, 1983, 62, 846–851. [PubMed: 6882926]
52. Amer J, Goldfarb A and Fibach E, Eur J Haematol, 2003, 70, 84–90. [PubMed: 12581189]
53. Daghman N, Elder G, Savage G, Winter P, Lappin T and Maxwell A, Ann Hematol, 1999, 78, 275–278. [PubMed: 10422630]
54. Wang Y, Zheng Y, Zhang L, Wang Q and Zhang D, J Control Release, 2013, 172,1126–1141. [PubMed: 23954372]
55. Müller R, Jacobs and C Kayser 0, Adv Drug Deliv Rev, 2001, 47, 3–19. [PubMed: 11251242]
56. Pawar VK, Singh Y, Meher JG, Gupta S and Chourasia MK, J Control Release, 2014,183, 51–66. [PubMed: 24667572]
57. Torchilin V, Adv Drug Deliv Rev, 2011, 63,131–135. [PubMed: 20304019]
58. Yoo J-W, Chambers E and Mitragotri S, Curr Pharm Des, 2010, 16, 2298–2307. [PubMed: 20618151]
59. Rodriguez PL, Harada T, Christian DA, Pantano DA, Tsai RK and Discher DE, Science, 2013, 339, 971–975. [PubMed: 23430657]
60. Nakanishi T, Kunisawa J, Hayashi A, Tsutsumi Y, Kubo K, Nakagawa S, Nakanishi M, Tanaka K and Mayumi T, J Control Release, 1999, 61, 233–240. [PubMed: 10469918]
61. Hu C-MJ, Fang RH, Luk BT, Chen KN, Carpenter C, Gao W, Zhang K and Zhang L, Nanoscale, 2013, 5, 2664–2668. [PubMed: 23462967]
62. Kim DD, Miwa T, Kimura Y, Schwendener RA, van Lookeren Campagne M and Song W-C, Blood, 2008,112, 1109–1119. [PubMed: 18524992]
63. Fang RH, Hu C-MJ and Zhang L, Expert Opin Biol Ther, 2012, 12, 385–389. [PubMed: 22332936]
64. Muzykantov VR, Murciano JC, Taylor RP, Atochina EN and Herraez A, Anal Biochem, 1996, 241,109–119. [PubMed: 8921172]
65. Laurencin M, Cam N, Georgelin T, Clément O, Autret G, Siaugue JM and Ménager C, Adv Healthc Mater, 2013, 2, 1209–1212. [PubMed: 23568859]
66. Wang C, Sun X, Cheng L, Yin S, Yang G, Li Y and Liu Z, Adv Mater, 2014, 26, 4794–4802. [PubMed: 24838472]
67. Pan D, Vargas-Morales O, Zern B, Anselmo AC, Gupta V, Zakrewsky M, Mitragotri S and Muzykantov V, PloS one, 2016, 11, e0152074. [PubMed: 27003833]
68. Pan DC, Myerson JW, Brenner JS, Patel PN, Anselmo AC, Mitragotri S and Muzykantov V, Sci Rep, 2018, 8, 1615–1627. [PubMed: 29371620]
69. Muzykantov VR, Expert Opin Drug Deliv, 2010, 7, 403–427. [PubMed: 20192900]
70. Müller K, Fedosov DA and Gompper G, Sci Rep, 2014, 4, 4871–4879. [PubMed: 24786000]
71. Lee T-R, Choi M, Kopacz AM, Yun S-H, Liu WK and Decuzzi P, Sci Rep, 2013, 3, 2079–2087. [PubMed: 23801070]

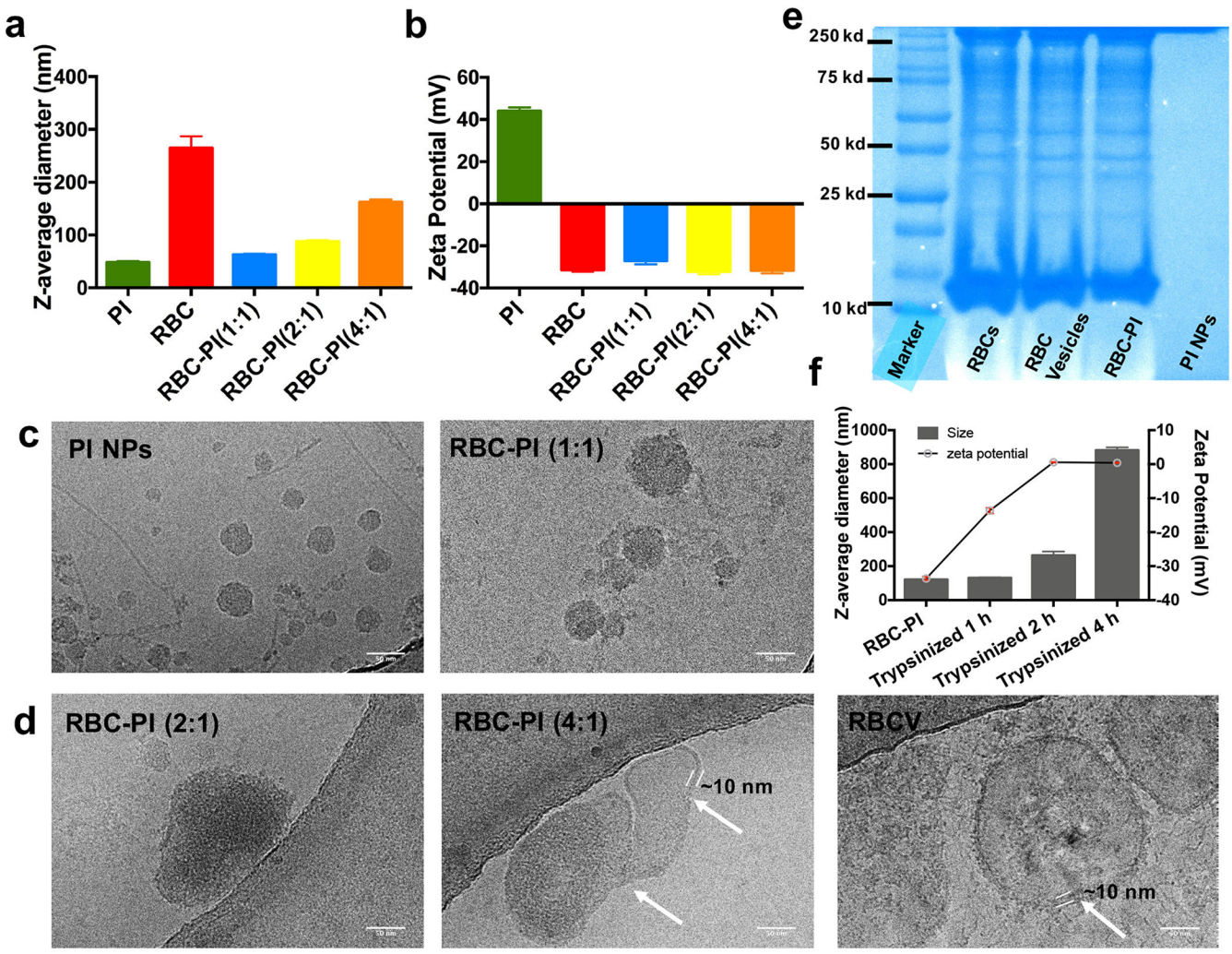

Figure 1.

a) Size distribution, and b) zeta potential of the RBC vesicles to PI complexed nanoparticles at different ratios. c) Cryo-electron microscopy images of PI NPs and RBC-PI (1:1); and d) various RBC vesicles-to-PI ratios (2:1, 4:1) and RBC vesicles. Arrows indicated RBC bi-layered cell membrane. Scale bar = 50 nm; e) SDS-PAGE protein analysis of RBCs, RBC vesicles, RBC-PI (1:1) and PI NPs. f) Sizes and zeta potential of RBC-PI before and after trypsinization. Trypsinization resulted in the loss of particle stability.

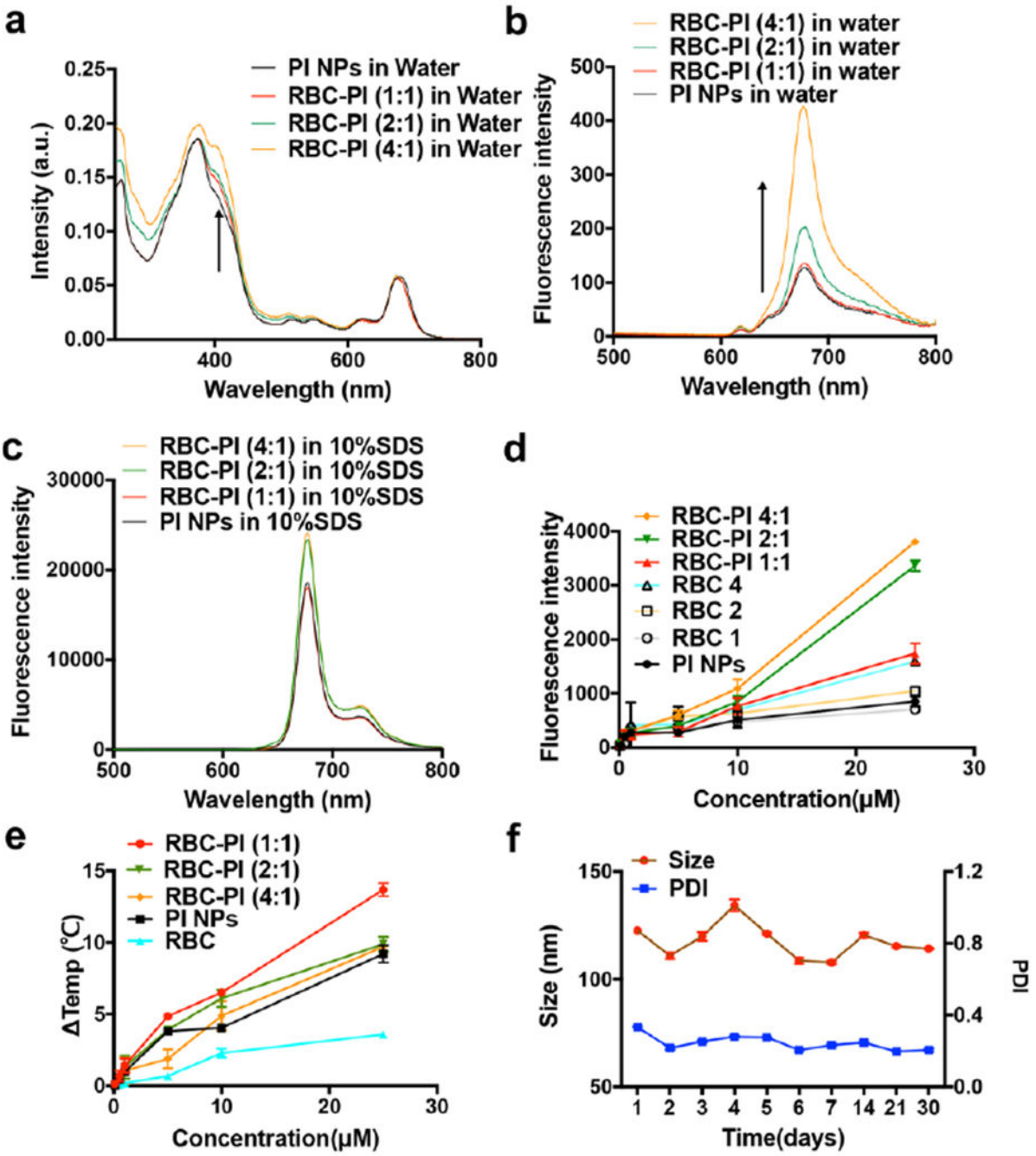

Figure 2.

a) UV-Vis absorbance of PI NPs and RBC-PI with various RBC vesicles-to-PI ratios in water; Fluorescence spectra of PI NPs and RBC-PI with various RBC vesicles-to-PI ratios in water b) and 10% SDS c) with excitations of 412 nm (PI concentration: 50 nM); d) ROS generation of RBC-PI with various RBC vesicles -to-PI with different ratios upon irradiation (680 nm at 0.8 W/cm^2 for 3 min); e) Quantitative temperature increases of RBC-PI with various RBC vesicles -to-PI ratios, PI NPs and RBC upon illumination (680, 0.8 W/cm^2, 3

min); f) Stability test of RBC-PI (RBC vesicles-to-PI ratio: 1:1) in the presence of 10% FBS/PBS under 37 °C for 30 days. Size and PDI were measured by DLS.

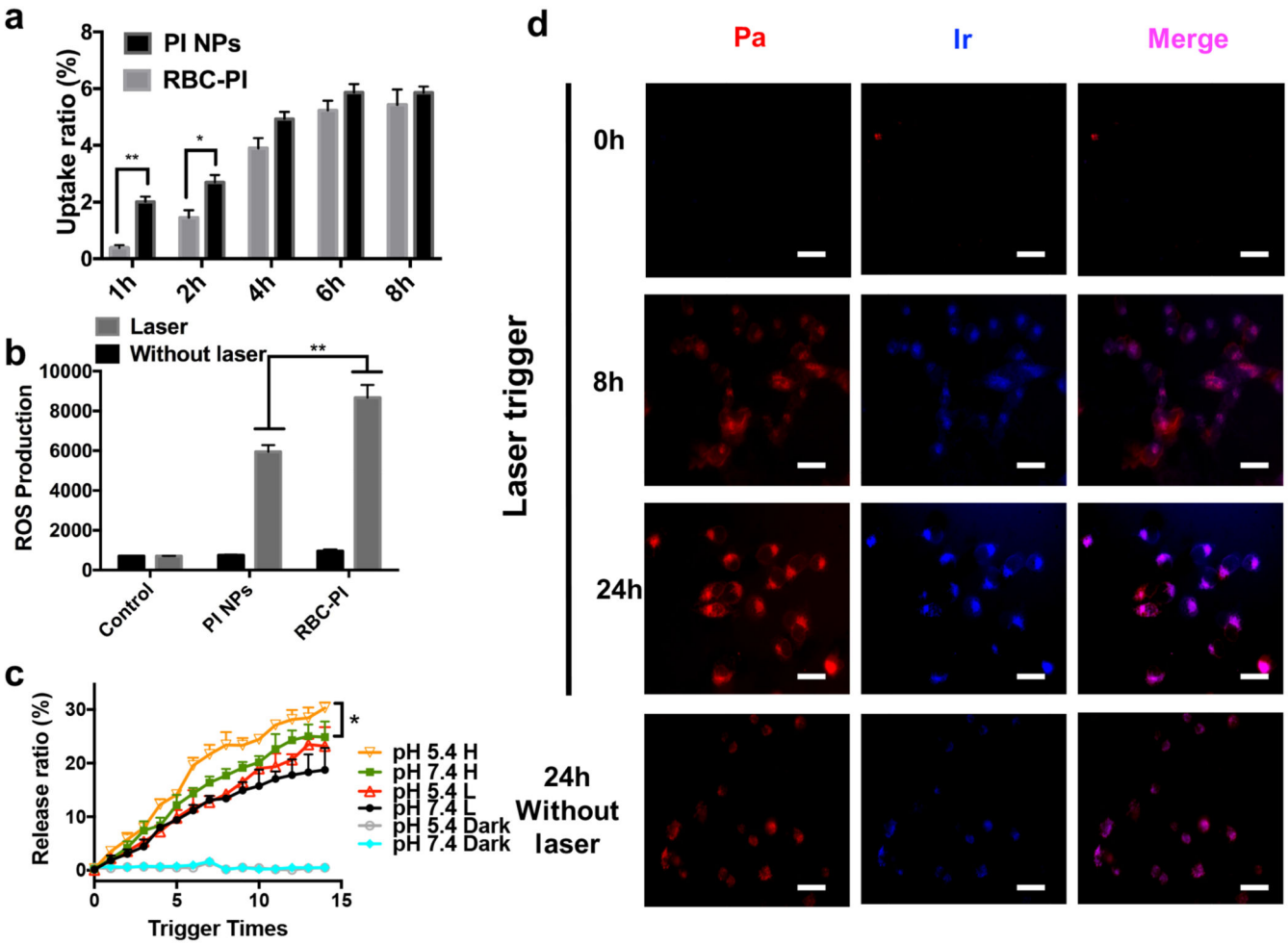

Figure 3.

Uptake and photo-chemotherapy in A549 human lung cancer cells. a) intracellular uptake of RBC-PI and PI NPs by A549 cells after 1, 2, 4, 6 and 8 h of incubation. b) intracellular ROS production of PI and RBC-PI with and without light treatment assessed with flow cytometry with DCF-DA as a ROS indicator; c) Light triggered drug release under pH 7.4 and 5.4 (mimicking lysosome pH). L: (0.8 W/cm^2 for 3 min); H: (1.6 W/cm^2 for 3 min); d) Self-indication of cellular behaviors and time-dependent drug release of RBC-PI (25 μM). Red: free Pa molecules or dissociated PI, Blue: cleaved Ir. Bar = 50 μm, (* P< 0.05, ** P<0.01).

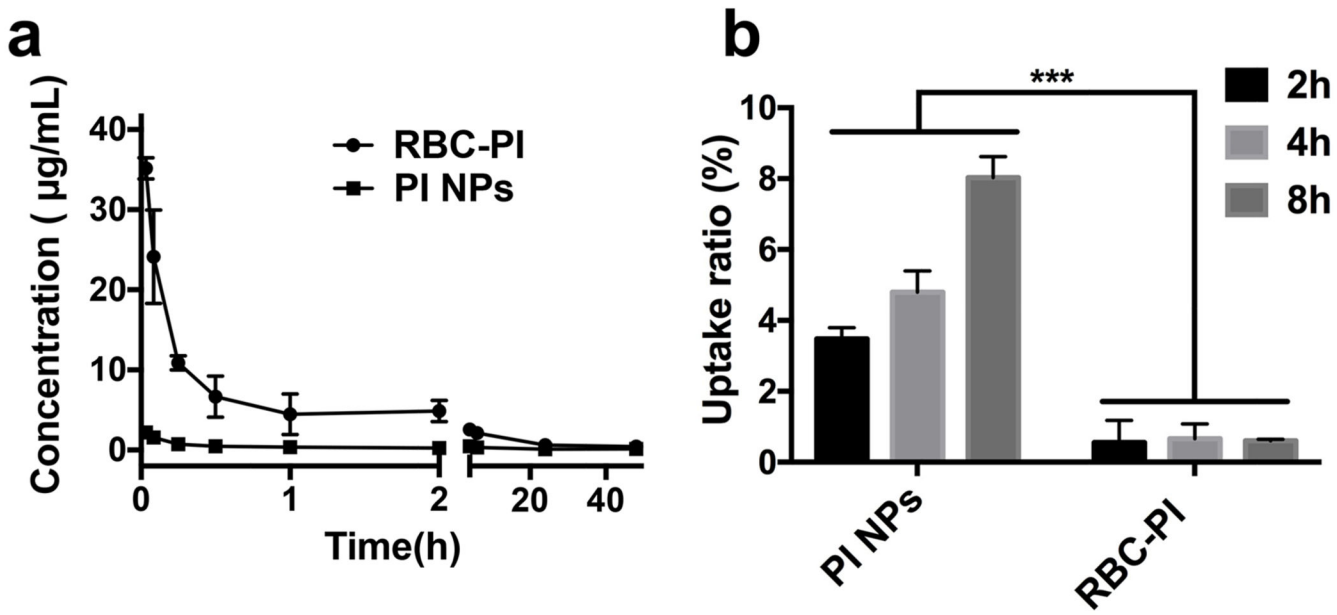

Figure 4.

a) Pharmacokinetic evaluations of RBC-PI and PI NPs (5 mg/kg) in rats (n=3). b) Intracellular uptake of RBC-PI and PI NPs by U937 human macrophage cells after 2, 4 and 8 h of incubation. (*** $P < 0.0001$).

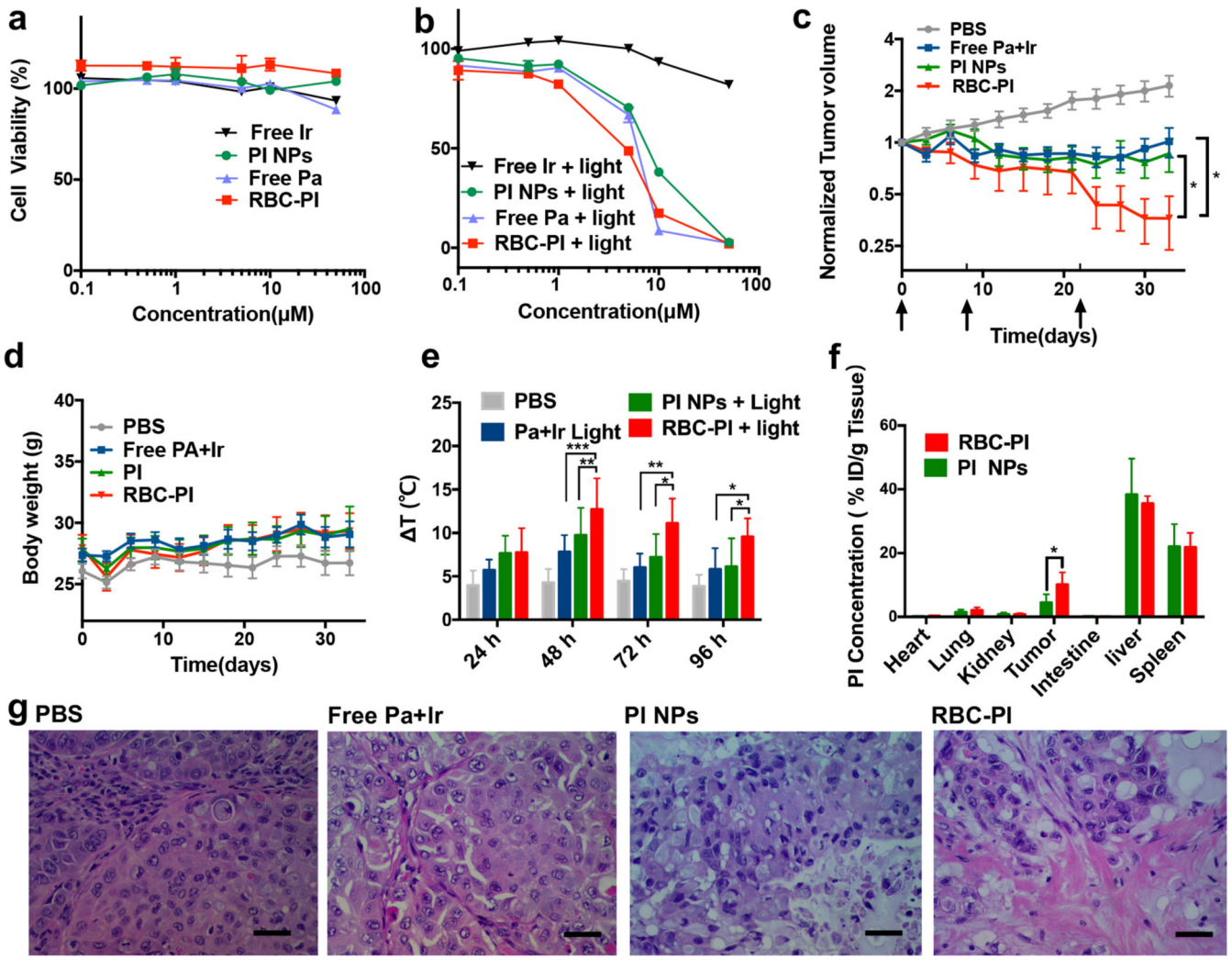

Figure 5.

Cell viability studies of free Pa, Ir, PI NPs and RBC-PI against A549 human lung cancer cells without a) or with b) laser treatments. Anti-cancer efficacy studies were performed in the A549 tumor-bearing mice; Tumor volume ratios c) and body weight d) changes of mice treated with PBS, mixture of Pa + Ir, PI NPs, and RBC-PI (equal to 10 mg/kg of Pa and 10 mg/kg of PI) on day 1, 7 and 21 followed by light treatments (n=6). Tumors were illuminated with 680 nm laser at 1.2 W for 3 minutes at 24, 48, 72, and 96 hours after each injection; e) Tumor surface temperatures at each different time point and group were monitored using NIR thermal camera; f) Biodistribution of PI and RBC-PI at 48 h after the injection. (* P< 0.05, ** P<0.01, *** P<0.001); g) Histopathological evaluations of A549 tumors upon PBS, Pa+Ir, PI NPs and RBC-PI mediated photochemotherapy, bar= 60 μm.

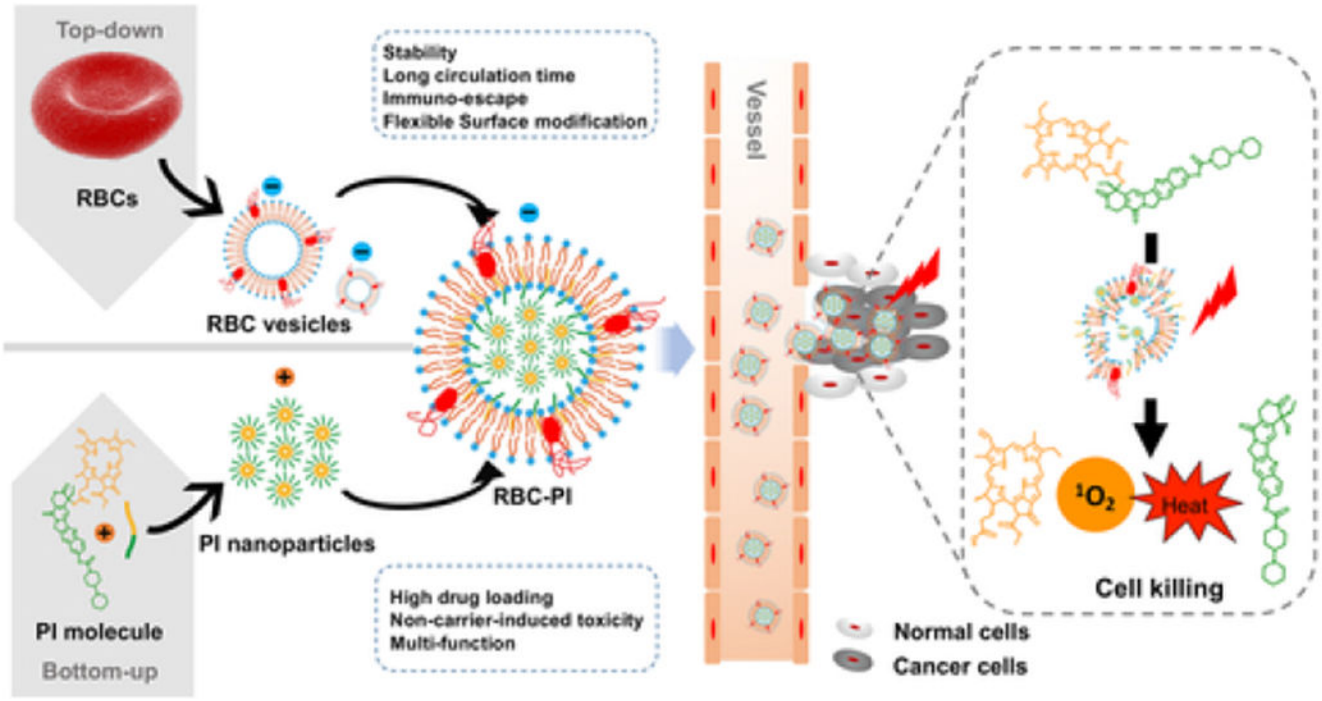

Scheme 1.

Schematic design of biomimicry FAPIN nanocomplex via synergistic combination of bottom-up and top-down approaches for cancer chemophototherapy. Positive surface charged nanoparticles self-assembled by Pa and Ir conjugate (PI) could complex with RBC derived membrane vesicles. RBC membrane modified biomimicry nanoparticles could prevent systemic macrophage clearance, and effectively accumulate at the tumor site via EPR effects allowing effective chemophotothearpy.